Interactions between polymer brushes and a polymer solution: mesoscale modelling of the structural and frictional properties

Florent Goujon,*[a] Patrice Malfreyt[b] and Dominic J. Tildesley[c]

Received 2nd February 2010, Accepted 8th April 2010
DOI: 10.1039/c002204g

We report mesoscopic simulations of polymer brushes in the presence of free polymer chains. We have used the dissipative particle dynamics method to model entangled polymer chains in a good solvent. We have studied the structure of the grafted and free chains under shear, as well as the dynamics of the detechment of polymer chains from the grafted surface. A comparison between entangled and nonentangled systems is presented. Entanglements are modeled using a bond repulsion potential. The rheology has been studied at different polymer grafting densities, in the presence of a varying number of free chains. We have shown that the detachment of grafted chains creates a central zone of free chains which exhibits a bulk like behaviour. The viscosity of this region is significantly increased compared to that of a polymer brush with the same grafting density and no detached chains. The presence of free polymer chains dramatically changes the friction coefficient. We have established that a fraction of detached chains of only 15% induces a decrease in the friction of 50%. This behaviour is correlated to the decrease of the interpenetration between the two opposing brushes. The detachment of chains from the surface, that may well occur at high sliding velocity in the surface force apparatus, is likely to have a significant effect on the observed experimental friction.

1 Introduction

A polymer brush consists of polymer chains which are end-grafted to a solid surface at high surface coverage. This leads to a dramatic change in the surface properties which are of great interest in many disciplines, such as biocompatibility, colloidal stabilization,[1–3] surface protection or modification.[4] A detailed understanding of the structure of the brush is necessary to understand these issues. Additionally, the mechanical and rheological properties of the brushes are of importance, because the presence of grafted chains can reduce the friction between two surfaces by three orders of magnitude.[5,6] Experiments involving the surface force apparatus[5–11] are the best way of studying interacting polymer brushes by measuring the normal and tangential components of the pressure under constraints. Those studies under compression and shear are a key to understand the lubrication process. The static properties of polymer brushes have also been studied extensively using SCF theories, which predict scaling laws for the structure and mechanical properties of polymer brushes.[12–17]

The simulation of polymer systems is made difficult because of the large time and length scales involved in such systems. Molecular methods using an all-atom description have been used to study the different regimes of polymer melts[18,19] as well as the structure of polymer brushes.[20,21,22] Recently, simulations at the mesoscopic scale have become a powerful tool to model large polymer systems: the soft interaction potentials and the thermostats used in these methods allow us to consider longer time scales. Polymer brushes have been successfully studied using various techniques such as stochastic dynamics,[23–30] dissipative particle dynamics[31–33] or Monte Carlo.[34,35] Some of those methods were used to study nonequilibrium systems, which is the case for polymer brushes under shear.

Dissipative particle dynamics (DPD) is a mesoscopic simulation method[36,37] which considers particles as virtual fluid elements. Consequently, the simulated time and length scales are much greater than in conventional molecular dynamics, but the interactions between such particles are soft, as the particles may overlap at this scale. We have used the DPD method in previous works to model polymer brushes in the presence of explicit solvent under compression and shear.[32,38,39] The model was recently improved by avoiding the topology violations between overlapping chains, which is a recurrent problem in mesoscopic methods using soft repulsive potentials.[40,41] Additionally, the dissipative and Brownian forces are short-ranged and pair-wise additive so that the dynamics obeys Newton's third law and the algorithm solves the Navier–Stokes equation for the system. This method properly includes the hydrodynamic interactions.

The interaction of a polymer brush in the presence of free chains is of great interest because of the change in the wetting properties of the surface, and has been widely studied using various theoretical and simulation methods.[42–50] In the case of the detachment of polymer chains from a highly grafted surface, the grafted layer expels the polymer into the solvent. The structure of the brush is not changed if the free chains are short because they behave like the solvent under shear flow. However, the desorption of long chains may cause a significant alteration of the brush structure and rheology. In the case of two

[a]*Laboratoire Thermodynamique et Interactions Moléculaires UMR CNRS 6272, Université Blaise Pascal, 63177 Aubière Cedex, France. E-mail: florent.goujon@univ-bpclermont.fr*
[b]*Laboratoire Thermodynamique et Interactions Moléculaires UMR CNRS 6272, Université Blaise Pascal, 63177 Aubière Cedex, France*
[c]*Unilever Research Port Sunlight, Bebington, Wirral, UK, CH63 3JW, United Kingdom*

polymer-coated surfaces interacting with each other, this results in an interface between grafted and free polymer chains. The dynamics of such detachment has been already studied by theory[51] and Monte Carlo simulations[52] using the bond-fluctuation model. The Monte Carlo results were discussed in terms of simple scaling ideas appropriate for a Rouse model and suggest a mechanism controlled by the entropy gain of the detached layers. These simulations used a coarse-grained description of the polymer chain by considering that 3 or 5 chemical monomers were integrated into one effective bond. However, the solvent particles were not treated explicitly. This can impact significantly the rheological properties of the grafted and detached chains.

In this work, we use the DPD method to model the effect of the detachment of polymer chains from two interacting grafted surfaces immersed in a good solvent. As the grafted and free chains are chemically identical and of same length, an entropic dewetting should be observed, forming a solution of free polymer chains in a good solvent. The brush/solution, which results from an interpenetration between the brushes and the free polymer chains, determines properties such as interfacial tension, pressure and structure. We focus on the change in structural and frictional properties of the polymer brushes in the presence of detached chains. Three major issues are discussed in this paper: how do the polymer chains behave once detached from the surface? What is the structure of the brush/solution interface? How does the presence of the polymer solution affect the frictional properties? In order to answer these questions, we have simulated polymer brushes systems at various grafting densities in the presence of free chains of identical length.

The paper is organized as follows: the first section details the DPD method and the model used for the simulation of the polymer brushes systems with and without free chains. The second section contains our results: the first part is a study of the structure at the brush/solution interface; the second part deals with the dynamics of the polymer chains after detachment; the third part describes the rheology of the system by studying the influence of free chains on the friction and viscosity. The third section contains our conclusions.

2 Simulation

2.1 The DPD model

The interactions between DPD particles at the mesoscopic scale are represented by the sum of three pairwise forces: a conservative force, a dissipative force and a random force. The conservative force $\mathbf{f}^C$ derives from a potential energy and gives the thermodynamic properties of the system. A simple soft force is used to model the repulsion between particles.[53]

$$\mathbf{f}_{ij}^C = \begin{cases} a_{ij}\left(1-\dfrac{r_{ij}}{r_c}\right)\hat{r}_{ij} & \left(r_{ij} < r_c\right) \\ 0 & \left(r_{ij} \geq r_c\right) \end{cases} \quad (1)$$

where r_c is the cutoff radius and $\hat{\mathbf{r}}_{ij}$ is the unit vector along the $i-j$ direction. a_{ij} is the maximum repulsion between particles i and j. The dissipative force $\mathbf{f}^D$ allows the particles to dissipate energy through a local friction parameter γ. The random force $\mathbf{f}^R$ models the Brownian motion by adding energy to the system:

$$\mathbf{f}_{ij}^D = -\gamma\omega^D(\hat{\mathbf{r}}_{ij}\cdot\mathbf{v}_{ij})\hat{\mathbf{r}}_{ij} \quad (2)$$

$$\mathbf{f}_{ij}^R = \sigma\omega^R\theta_{ij}\frac{1}{\sqrt{\delta t}}\hat{r}_{ij} \quad (3)$$

In these equations, θ_{ij} is a random number with gaussian distribution, zero mean and unit variance and $\mathbf{v}_{ij} = \mathbf{v}_i - \mathbf{v}_j$ is the difference between the velocities of particles i and j. ω^D and ω^R are weighting functions which are related to one another by the fluctuation–dissipation theorem: the DPD methods samples the canonical ensemble if the following conditions are satisfied[54]

$$\gamma = \frac{\sigma^2}{2k_BT} \quad \text{and} \quad \omega^D(r_{ij}) = \left(\omega^R(r_{ij})\right)^2 \quad (4)$$

where k_B is Boltzmann's constant and T is the imposed temperature. As no explicit form is imposed for the weighting functions, a simple soft repulsive expression has been chosen similar to the expression of the conservative force ($\omega_D = 1 - r_{ij}/r_c$).[53]

The forces are integrated using a modified velocity-Verlet algorithm. Reduced units are used through the paper: the mass of a DPD particle is taken as unity, as well as the cutoff radius r_c. Consequently, the reduced length is expressed as $r^* = r/r_c$. The unit energy ε is used to express the reduced temperature as $T^* = k_BT/\varepsilon$. We use an imposed temperature $T^* = 2.0$ in all of the simulations presented in this paper. The other reduced variables can then be deduced, so that the interaction parameter $a^* = a(r_c/\varepsilon)$, the unit of time $t^* = t(\varepsilon/mr_c^2)^{1/2}$ and the shear rate $\dot{\gamma}_a^* = \dot{\gamma}_a(mr_c^2/\varepsilon)^{1/2}$. Reduced units are a convenient tool for DPD, as the polymer particle may represent from one up to a dozen of monomers, depending on the interaction potential and the time step. As discussed by Groot and Rabone,[55] the time scale t^* is fixed by matching the diffusion constant of solvent. For the set of a_{ij} parameters used here, the timestep $\delta t = 0.01\ t^*$ is approximately 5 ps. As all the values presented here are in reduced units, the star notation is omitted in the following sections for clarity.

2.2 Polymer brushes

The accurate modeling of polymers using mesoscopic particles is an active field of research. Many authors have dealt with the issue of connecting the microscopic and mesoscopic scales to model different types of polymers.[56–60] In this work we model generic homopolymer chains to study the physics of the polymer brushes system. As any soft potential can give a correct description at the mesoscopic scale,[53] the simplest linear repulsion force given in eqn (1) is used in this article. A simple harmonic spring force between the beads is added[61,62] to connect particles i and j:

$$\mathbf{f}_{ij}^S = k_s(r_{ij} - r_{eq})\hat{\mathbf{r}}_{ij} \quad (5)$$

where k_s is the harmonic spring constant. The quality of the solvent is determined by the polymer–solvent interaction parameter $a_{\text{sol–sol}}$. Previous works have established[31,32] a set of interaction parameters to model polymer brushes: the reduced repulsion parameters are $a_{\text{pol–pol}} = a_{\text{sol–sol}} = 60.0$. A good solvent is then defined by a smaller value of $a_{\text{pol–sol}}$, taken to be 50.0 in this work.

The polymer model has been improved by adding a segment-repulsion force $\mathbf{f}^E$ to keep the entangled topology of the chains:[40,63,64]

$$\mathbf{f}_{ij}^{E} = \begin{cases} a_{ij}^{ent}\left(1-\dfrac{d_{ij}}{r_c^E}\right)\hat{d}_{ij} & \left(d_{ij} < r_c^E\right) \\ 0 & \left(d_{ij} \geq r_c^E\right) \end{cases} \quad (6)$$

where d_{ij} is the minimum distance between the two bond segments i and j. The parameters a_{ij}^{ent} and r_c^E are the entanglement interaction parameter and cutoff, respectively. The reduced values $a_{ij}^{ent} = 40.0$ and $r_c^E = 0.80$ have been used in previous work[40,41] and are a good compromise that avoids many topology violations without changing the nature of the interaction between the polymer and the solvent.

A typical simulation box consists of two solid surfaces grafted with polymer chains immersed in solvent particles. The surfaces are modeled using two layers of DPD particles tethered to an hexagonal lattice using an harmonic potential. The brushes are formed by randomly connecting one end of each polymer chain to surface particles. The total number of chains is equally distributed on the two surfaces so that each brush has the same grafting density. Fig. 1 shows a schematic view of such a system, in which the z direction is chosen as the normal to the surfaces.

A shear rate is applied to the system by imposing a movement on the surface particles along x-axis. The amount δx is added to the reference lattice:

$$\delta x = \pm\frac{\dot{\gamma}_a L_z}{2}\delta t \quad (7)$$

where $\dot{\gamma}_a$ is the shear rate, L_z is the inner distance between the surfaces and $\delta t = 0.01$ is the timestep used in all the simulations. The sign depends on which surface is considered, as they slide along opposite directions.

2.3 System

Each system consists of two 27×12 hexagonal layers separated by a distance $L_z = 17.0$. With an imposed distance $d_w = 0.617$ between two wall particles, the size of the simulation box along the xy plane is 16.659×9.618 in reduced units. A polymer chain is $N_b = 20$ beads long, and can be either grafted onto a surface or free in the system. A series of 11 simulations were performed with an increasing number of free chains. In the detached systems (see Table 1), the free chains are provided by the detachment of a number of chains N_f from each surface. Additionally, solvent particles are added randomly in the box: a number of solvent $N_s = 3500$ is chosen which gives a total density $\rho = 3.4$ between the surfaces. The polymer grafting density is defined by ρ_a which represents the average number of grafted chains per reduced surface area.

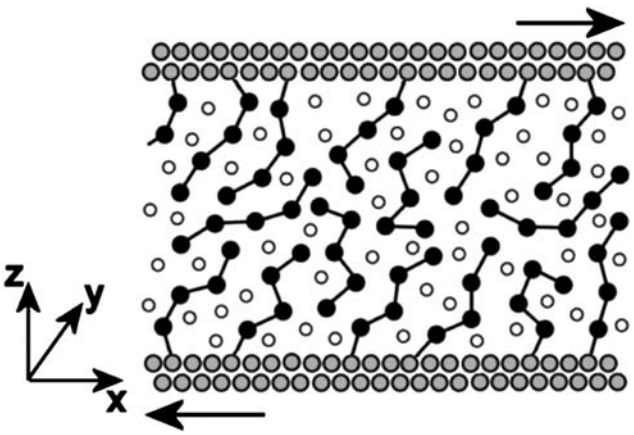

Fig. 1 A schematic view of the simulated system. Grey circles are the wall particles tethered to a two-layers hexagonal lattice, black circles represent the polymer chains, and white circles represent solvent particles. The two arrows show the direction of the imposed shear movement of the surfaces along the x-axis.

Table 1 Summary of the simulated systems. N_g is the number of grafted polymer chain on each surface, and ρ_a is the corresponding grafting density. N_f and N_s are the number of free chains and solvent particles in the box. As reference systems contain no free chains, the number of solvent particles $< N_s >$ is adjusted so that the solvent chemical potential is the same in all reference systems

		Detached systems		Reference systems	
N_g	ρ_a	N_f	N_s	N_f	$<N_s>$
146	0.911	0	3500	0	3500
136	0.845	20	3500	0	3893
126	0.787	40	3500	0	4302
116	0.724	60	3500	0	4687
106	0.662	80	3500	0	5086
96	0.560	100	3500	0	5483
86	0.537	120	3500	0	5882
76	0.474	140	3500	0	6271
66	0.412	160	3500	0	6654
56	0.350	180	3500	0	7054
46	0.287	200	3500	0	7435

A typical run is as follows: the simulation box is equilibrated under shear with the maximum number of grafted chains (146 on each wall). Some of these chains are then detached during a second run of length 200 000 timesteps. The chains are detached at regular intervals during the first half of the simulation, alternating from the top and bottom wall ($N_f/2$ chains are then detached from each surface). The dynamics of the detachment is studied during this simulation. Once all the detached chains have reach their equilibrium position, an acquisition of length 300 000 timesteps is performed. The structural and rheological properties are calculated during this run by averaging over 3000 configurations, saved every 100 timesteps. Fig. 2 shows

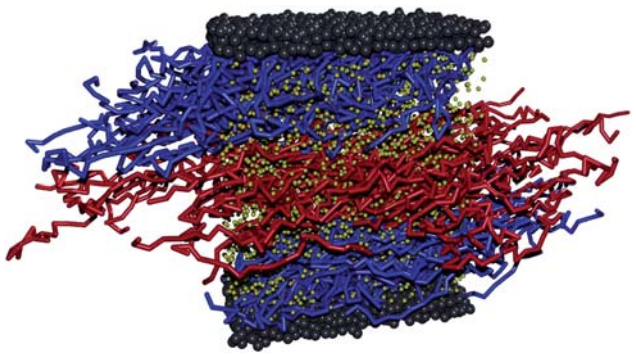

Fig. 2 Snapshot of a simulation box with $\rho_a = 0.724$ and 60 detached chains at equilibrium. The grafted and free polymer chains are shown in blue and red, respectively, solvent is shown in yellow.

a configuration of the detached system with $\rho_a = 0.724$ during the acquisition process.

In order to study the influence of free chains only, we have to compare each system with an other one which contains the same number of grafted chains on the surface. Those systems are called reference systems (see Table 1), and contain no free chains. As the total number of polymer particles is different in each reference system, the number of solvent particles must be adjusted to keep the solvent chemical potential constant in all the reference systems. The local configurational chemical potential of the solvent μ^{conf} is calculated in the system with $\rho_a = 0.911$ (all chains grafted) using the test-particle insertion method[65–68]

$$\mu^{\text{conf}}(z) = k_B T \ln\left[\frac{\langle\rho(z)\rangle_{\text{NVT}}}{\left\langle\exp(-\frac{\Delta U^{\text{test}}}{k_B T})\right\rangle_{\text{NVT}}}\right] = k_B T \ln\langle Z(z)\rangle_{\text{NVT}} \quad (8)$$

where $\rho(z)$ is the local solvent density. The value of μ^{conf} is then used in the simulation to adapt the number of solvent particles by performing hybrid dynamics: the constant-μVT ensemble is sampled by attempting Monte Carlo moves for creation/deletion of solvent particles. Every 500 timesteps, the program attempts to create or delete a solvent particle using the following acceptance probabilities:

$$P^{\text{acc}}_{\text{creation}} = \min\left[1, \frac{\langle Z\rangle_z V}{N+1}\exp\left(-\frac{\Delta U}{k_B T}\right)\right] \quad (9)$$

$$P^{\text{acc}}_{\text{deletion}} = \min\left[1, \frac{N}{\langle Z\rangle_z V}\exp\left(-\frac{\Delta U}{k_B T}\right)\right] \quad (10)$$

where $Z = \exp(\mu_{\text{conf}}/k_B T)$ is the imposed activity of the solvent. Further details of a DPD simulation in the grand canonical ensemble can be found in our previous papers.[38,39] A simulation of a reference system is as follows: an equilibration of length 500 000 timesteps is run in order to adjust the number of solvent particles. The analysis are then done during a 300 000 timestep acquisition. Both simulations are run at constant chemical potential, which gives the average number of solvent particles $< N_s >$ given in Table 1. The imposed value of the solvent chemical potential, calculated from the system with highest grafting density ($\rho_a = 0.911$) is $\mu_{\text{conf}} = 19.8$ in reduced units. The fluctuations for $< N_s >$ are approximately $\pm$ 10 particles in any simulation.

3 Results and discussions

3.1 Structure

We have calculated the local density profile $\rho(z)$ along the normal z-axis for the different types of polymer beads (grafted or free). Fig. 3 shows the $\rho(z)$ profiles for three systems containing increasing amounts of free chain: $\rho_a = 0.911$ (no free chains), $\rho_a = 0.662$ (80 free chains) and $\rho_a = 0.412$ (160 free chains). As expected, the detached chains form a central phase, which grows with the addition of free chain. The brushes shrink as more chains are detached in order to keep the average polymer density constant through the box. The brush profiles are different in the case of the reference systems (grey curves in Fig. 3). In the reference systems, the missing chains are replaced by solvent particles, which allow the brushes to extend in the direction

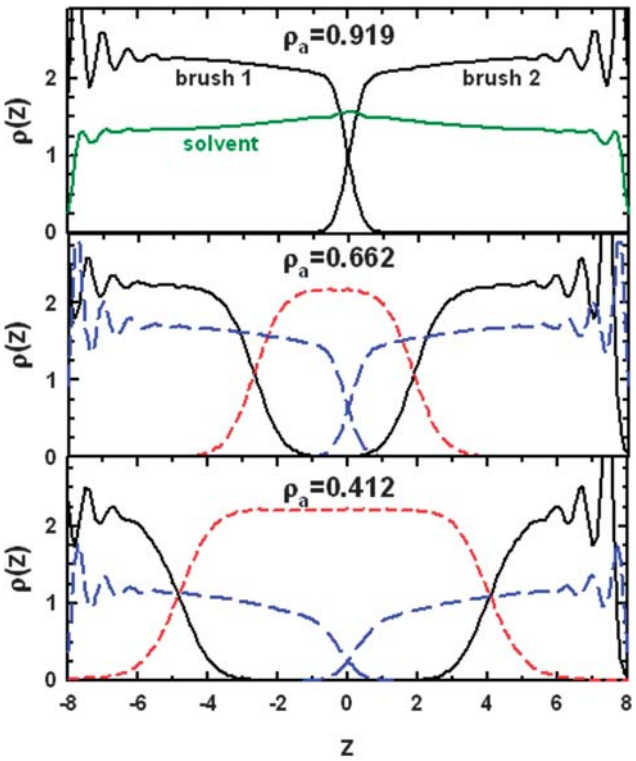

Fig. 3 Number density profiles for polymer chains as a function of z: system with no free chains ($\rho_a = 0.911$, top), system with 80 free chains ($\rho_a = 0.662$, middle), system with 160 free chains ($\rho_a = 0.412$, bottom). The solid and dashed curves represent the grafted and free chains, respectively.

normal to the surface. Additionally, the profiles are more step-like when no free chains are present. The brush height h is calculated from the first moment[21]

$$h = 2\frac{\int_{-L_z/2}^{L_z/2} z\rho_1(z)dz}{\int_{-L_z/2}^{L_z/2} \rho_1(z)dz} \quad (11)$$

where $\rho_1(z)$ is the average number density profile of one brush. Because the system is symmetric, both brushes have the same height, and the average value is plotted in Fig. 4. In this plot, the dependence of the height of the reference systems with grafting densities is also shown. The brush height does not change significantly in the reference systems as the brush regime is still maintained at the lowest grafting density. This means that additional solvent particles are created at constant-μ (see $< N_s >$ in Table 1) which fill the brushes in order to maintain the swollen state. This behaviour is well-known[13,14] and the brush height follows a scaling law $h \sim \rho_a{}^{1/3}$, shown in the figure for comparison. If the polymer brushes with the same grafting density are in contact with free chains, the polymer solution region does not allow the brushes to overlap. Consequently, the brush height is linearly dependant on the number of free chains. The detachment of polymer chains has a significant influence on the brush structure.

The depth of penetration of the polymer solution, λ inside the brush can be compared to theory. λ is calculated from the density

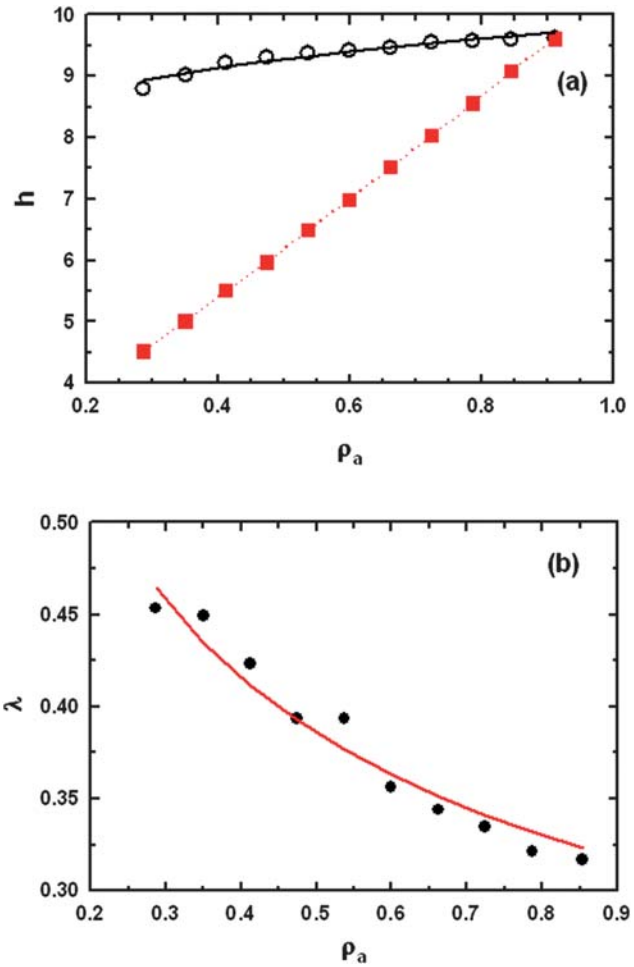

Fig. 4 (a) Brush height h as a function of the grafting density ρ_a in the middle of the box. Open circles represent the reference systems, in which the missing polymer chains are replaced by solvent particles (see section 2.3). (b) Penetration length of the polymer solution inside the brush λ as a function of ρ_a.

profiles as the difference between the maximum z coordinate of the brush profile and the minimum z coordinate of the profile of free chains. Both coordinates are chosen such that $\rho(z)$ is 5% of the maximum density. From symmetry, both brush/solution interfaces give a similar value for λ. Fig. 4b shows λ as a function of the grafting density. In the autophobicity regime (chemically identical chains of same length), theoretical predictions suggest the following scaling law[69,70]

$$\lambda \sim \rho_a^{-1/3} \tag{12}$$

Our results are in good agreement with eqn (12) (solid curve in Fig. 4b). As ρ_a decreases, the brushes become more permeable to the free central chains, resulting in an increase in λ.

3.2 Dynamics of the detachment

The dynamics of free chains has been studied in the case of 30 detached chains from each wall ($\rho_a = 0.724$). As each chain is detached at a different time, it is useful in averaging to consider a relative timescale. For each chain, the time origin is set at 20 000 timesteps before its detachment. At depletion, the harmonic spring which constrains the head of the polymer chains is removed, and the chain dynamics is studied during the following 80 000 timesteps.

Fig. 5a shows the time evolution of the position along z-axis for the centre-of-mass and the two ends of the detached chains. As $z = 0$ is the middle of the box, we use $-z_i$ for chains detaching from bottom wall for meaningful averaging. We can see that the chains are in a steady state before detachment, as the position of the center of mass and the tail bead does not change along z. Once the chains are in the central region the tail and head are indistinguishable. Once the chains are detached, they immediately diffuse to the central zone. The free chains are then ejected from the brush and are immersed in the central solvent region to form a polymer solution. It is interesting to note that once the chains have reached their equilibrium region, the average

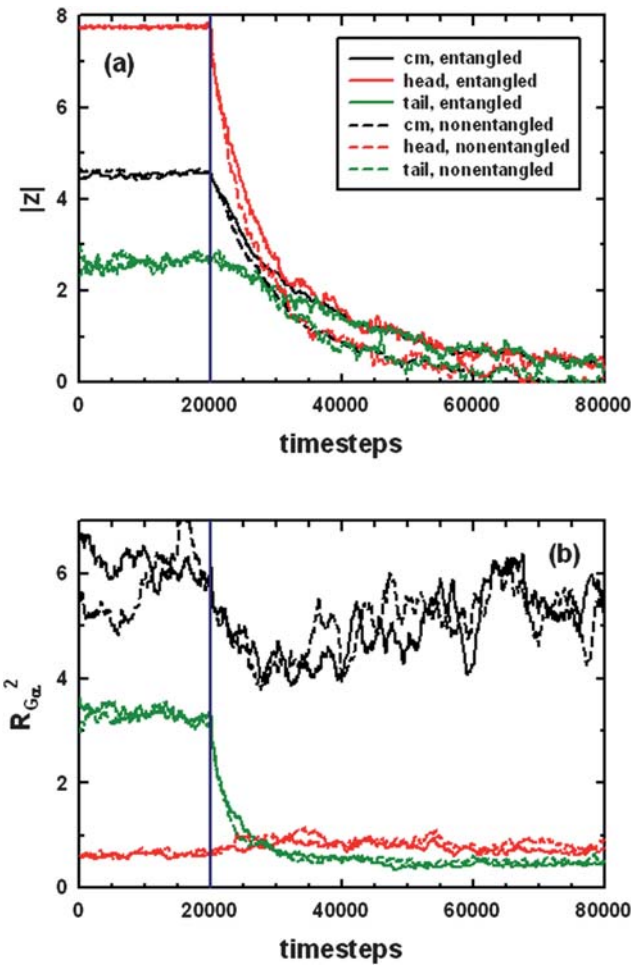

Fig. 5 (a) Evolution of the z coordinate of the position of polymer chains during the detachment process. Black curves show the position of the center-of-mass (cm), red curves show the position of the grafted end (head) and green curves show the position of the free end (tail). (b) Evolution of the radius of gyration of polymer chains. Black, red and green curves show the x, y and z components of the square radius of gyration R_G^2, respectively. For both (a) and (b), the time scale is adjusted for each chain so that the detachment occurs after 20 000 timesteps (shown as the vertical line). The average is performed on 60 detached chains ($\rho_a = 0.724$). Solid and dashed lines represent the simulations with and without entanglement forces, respectively.

z position of each head is the same. The head and tail beads in the free chains can not be distinguished. Binder *et al.*[52] have observed the same behavior and have divided the chain motion into two parts. At early times, the detached chains cross the polymer phase at constant velocity: in the present work this occurs in the first 10 000 timesteps, which correspond to approximately 50 ns. In a second period, when the chain has lost the memory of its grafting orientation, the motion is diffusive and the chain velocity is then proportionnal to $\sqrt{t}$. The time for the loss of memory is identified as the time when the two ends of the chain become equivalent.

We have also performed the same simulation ($\rho_a = 0.724$) using no bond repulsions. The dynamics without entanglements is represented by the dashed curves on the same figure. Interestingly, we observe that the trajectory of the detached chains is only slightly different. The dynamics of the detachment does not seem to be affected by the presence of entanglements. The polymer chains in the brush under shear is highly organized and each chain has an excluded volume whose shape is close to a cylinder. Thus, even without bond repulsions, a detached chain follows a trajectory which is governed by the reptation through the polymer brush and does not have significant entanglement interactions with its neighbours. In contrast, the average z coordinate is higher for entangled chains once they have reached the central region. This is due to the fact that the detached chains removed last from the walls can diffuse less in the central polymer solution due to the bond repulsions.

In order to investigate the structure of the chains during the detachment process, we have plotted the time evolution of the different components of the chain radius of gyration in Fig. 5b. Considering all particles have unit mass, the α component of the mean squared radius of gyration is

$$\left\langle R_{G\alpha}^2 \right\rangle = \frac{1}{N_p}\left\langle \sum_{i=1}^{N_p}\left(r_{i,\alpha} - r_{\mathrm{cm},\alpha}\right)^2 \right\rangle \tag{13}$$

where N_p is the number of beads in the polymer chain and $r_{i,\alpha}$ is the α component of the position of particle i (cm holds for center of mass). As observed in our previous paper,[32] the grafted chains are elongated along the direction x of the shear. During the detachment, the z component decreases very quickly. The free chains are only dependant on the shear flow, which continues on stretching the chains along the x direction. The change in the shape of detached chains is very fast compared to the time necessary for them to reach the central region. This means that once a chain is detached, its orientation is mainly along the shear flow. This period corresponds to the first part of the detachment process, during which the chain is losing the memory of its grafted shape. Then the chains diffuse across the moving brush and are expelled to the center of the box. This diffusion does not involve a change in the average shape of the chain. The transition between the grafted state and the solution state occurs over a 20 000 timesteps period (see Fig. 5b). This time can be compared with the orientational and shape relaxation times (τ_1 and τ_2, respectively). τ_1 is calculated from the rotational order parameter time correlation function $C_1(t)$

$$C_1(t) = \frac{1}{n_{t_0}\, N_c}\sum_{i=1}^{N_c}\sum_{j=1}^{n_{t_0}} \hat{\mathbf{e}}_i(t)\cdot\hat{\mathbf{e}}_i(t_0(j)) \tag{14}$$

where N_c is the total number of polymer chains, n_{t0} is the number of origin times and $\hat{\mathbf{e}}_i(t)$ is the normalized first eigenvector of the inertial tensor. τ_2 is calculated using the position autocorrelation function $R(t)$ of polymer chains

$$R(t) = \frac{1}{n_{t_0}\, N_c\, N_b}\sum_{i=1}^{N_c}\sum_{j=1}^{n_{t_0}}\sum_{k=1}^{N_b}\left[\mathbf{r}_{i,k}(t) - \mathbf{R}_{\mathrm{cm,i}}(t)\right]\cdot\left[\mathbf{r}_{i,k}(t_0(j)) - \mathbf{R}_{\mathrm{cm,i}}(t_0(j))\right] \tag{15}$$

where N_b is the number of beads in the polymer chain, $\mathbf{r}_{i,k}$ denotes the position of bead k in chain i and $\mathbf{R}_{\mathrm{cm,i}}$ is the position of the centre of mass of chain i. τ_1 and τ_2 are obtained by fitting $C_1(t)$ and $R(t)$ as $\exp(-t/\tau)$, respectively. The simulation used to calculate τ_1 and τ_2 consists of a bulklike phase containing free polymer chains and solvent particles at the same density than in the grafted system. τ_1 and τ_2 are 7500 timesteps and 14 500 timesteps, respectively. As a result, the detachment time in good solvent conditions is of the same order of magnitude as the time required for a free chain in solution to loose the memory of its shape and orientation. As a comparison, such relaxation times have been measured by using the fluorescence depolarization method. Depending on the molar concentration of polymer segments, the orientational relaxation time for polystyrene chains can vary from 5 to 10 nanoseconds.[71] Provided that the timestep δt is approximately 5 ps, τ_1 and τ_2 correspond in real units to 37 ns and 72 ns, respectively. Since the orientational relaxation time of a free polymer chain is the one comparison that we can make with experiment, the study of the detachment phenomenon would be a particularly useful experimental investigation.

The energy contributions acting on a polymer chain may vary during the detachment process. Fig. 6 shows the instantaneous potential energy of the detached chains as a function of time,

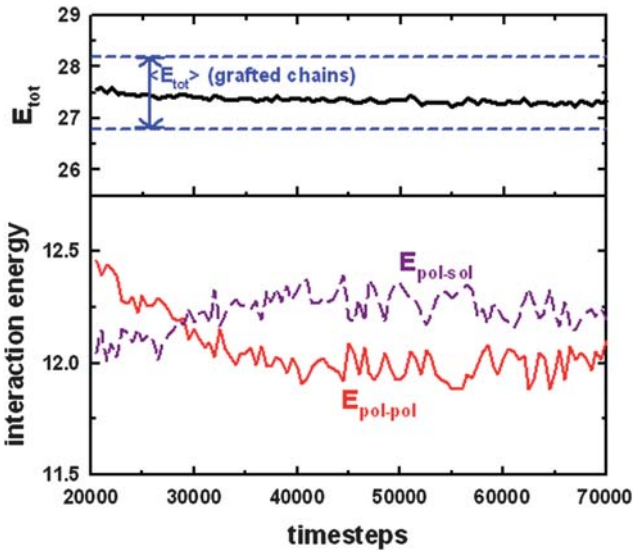

Fig. 6 Average interaction energy of the detached chains as a function of time for the system with grafting density $\rho_a = 0.474$. The time scale is adjusted for each chain so that the detachment occurs at timestep 0. The total potential energy (top) and the polymer–polymer and polymer–solvent conservative contribution (bottom) are shown.

starting from the detachment of each chain. The timescale used in this figure is the same as in Fig. 5. The total energy can be split into polymer–polymer and polymer–solvent energy contributions, calculated using the conservative potential of eqn (1). The polymer–polymer contribution decreases as the chain leaves the brush region. As the total density is constant in the simulation cell, the middle of the cell is filled by solvent particles, which obviously explains the increase of the polymer–solvent energy contribution at the same time. The upper part of Fig. 6 shows the evolution of the total interaction energy of the detached chains. The two dashed lines represent the extreme values of the average total energy of the grafted chains. Despite the change in the different types of energy contributions, we see that the total interaction energy of the detached chains remains the same as that of the grafted ones. Thus, the detachment is not governed by enthalpy but rather by entropic effects in a good solvent. The free chains in the polymer solution adopt a bulk-like behaviour in contrast to the grafted chains: this is then more favorable from an entropic viewpoint. These results are in good agreement with the theoretical models[72] and experiments.[69]

3.3 Frictional properties

The dependence of the brush structure on the presence of free chains may affect the rheological properties of the system. We have calculated the profiles of the components of the pressure tensor[73,74] along z-axis

$$p_{\alpha\beta}(z) = \rho(z)k_BT_{\alpha\beta}(z) - \frac{1}{L_xL_y}\left\langle \sum_i \sum_{j>i} \frac{(r_{ij})_\alpha (f_{ij})_\beta}{|z_{ij}|}\theta\left(\frac{z-z_i}{z_{ij}}\right)\theta\left(\frac{z_j-z}{z_{ij}}\right)\right\rangle \quad (16)$$

where $\mathbf{f}_{ij} = \mathbf{f}^C_{ij} + \mathbf{f}^D_{ij} + \mathbf{f}^R_{ij}$ is the total force acting between particles i and j, $\theta(x)$ is the unit step function which is 1 when $x > 0$ and zero otherwise. $< \ldots >$ denotes a configurational average, α and β represent the x, y or z coordinates. The double sum is over all pairs of interacting particles. $T_{\alpha\beta}(z)$ is the profile along z-axis of the $\alpha\beta$ component of the temperature tensor calculated from the velocities. Further details concerning the calculation of this property are given elsewhere.[32] The entanglement contribution to the pressure can be included by considering each pair of interacting segments.[40] The calculation of the local pressure allows us to check the mechanical equilibrium inside the simulation cell: the normal pressure $p_N = p_{zz}$ must be constant through the simulation cell for a planar interface.

Fig. 7a shows the profile of the tangential pressure $p_T(z) = \frac{1}{2}(p_{xx}(z) + p_{yy}(z))$ for various grafting densities. It is interesting to note that the brush system with no free chains ($\rho_a = 0.911$) exhibits a local tension between the brushes, as $p_T(z)$ is not constant. Due to the fact that the polymer solution becomes more developed, the interaction between the two opposite brushes weakens. This results in a decrease of the interfacial tension within the system. As a consequence, the presence of the polymer solution reduces the tension between the interacting polymer brushes.

The calculation of the xz component of the pressure p_{xz} is used to calculate rheological properties. The friction coefficient is defined by the ratio of tangential and normal pressure:[75]

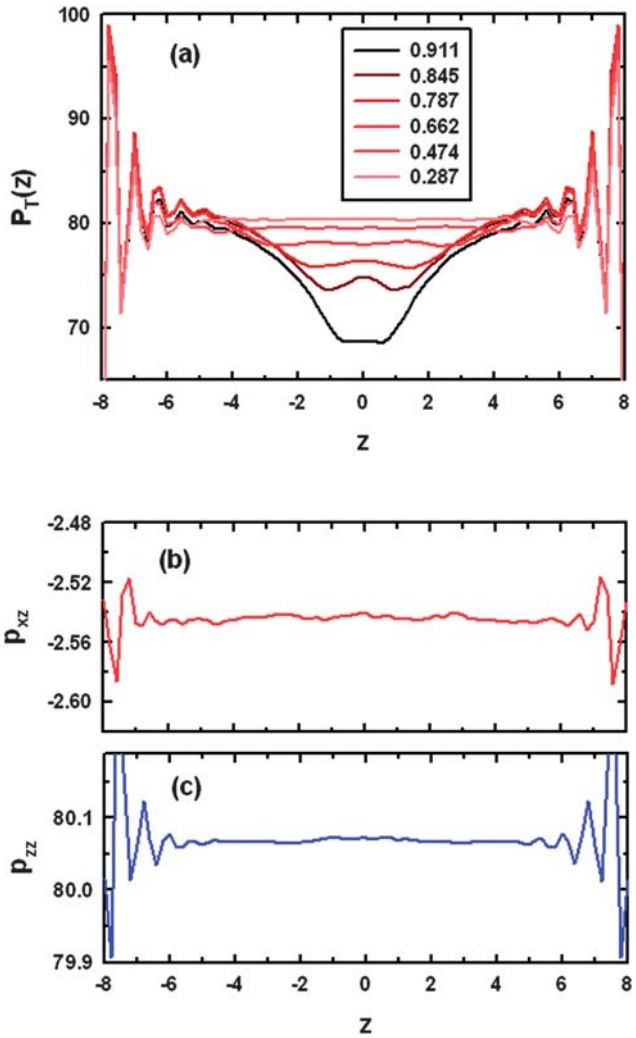

Fig. 7 (a) Profile of the tangential pressure along z-axis for systems containing various numbers of free chains. (b/c) Profiles along z-axis of the zz (b) and xz (c) components of the pressure tensor for a system with 60 free chains ($\rho_a = 0.724$).

$$\varepsilon(z) = -\frac{\langle p_{xz}(z)\rangle}{\langle p_{zz}(z)\rangle} \quad (17)$$

Fig. 7b shows the profiles of the xz and zz components of the pressure involved in the calculation of the friction. As the system is under shear, p_{xz} is not zero, but both values are constant through the simulation box. This gives an homogeneous profile for the friction. In Fig. 8 we report the mean value of the friction as a function of the surface coverage.

Firstly, the friction decreases almost linearly with the surface coverage in the reference system. As the structure of the brush does not change significantly with the surface coverage, the overlap region between brushes remains high. By contrast, free chains in the middle of the cell dramatically decrease the friction in the detached systems. In the case of 40 free chains (20 detached chains per wall, 14% of the grafted chains), the friction coefficient is decreased by almost 50%. This can be explained by the fact that the detached chains are expelled from the brushes due to the brush autophobicity. The free chains then form a central bulk

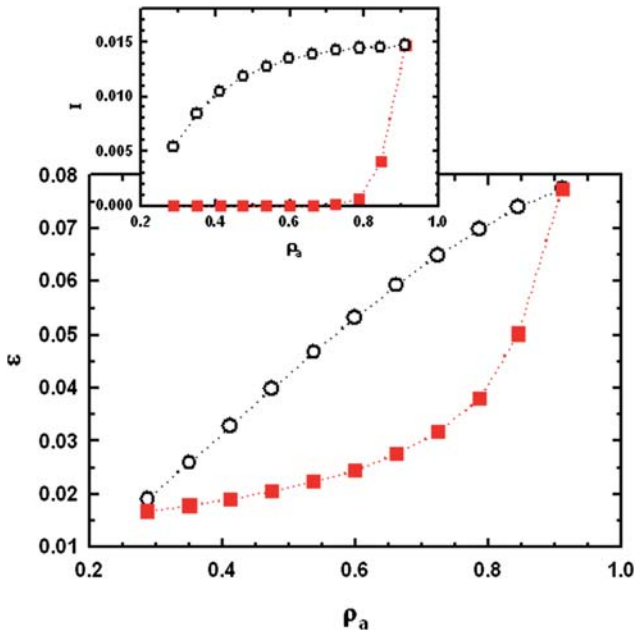

Fig. 8 Friction coefficient ε as a function of the grafting density ρ_a. Open circles represent the reference systems, in which the missing polymer chains are replaced by solvent particles (see section 2.3). The inset shows the evolution of the brush interpenetration I for the same systems.

phase which separates the two brushes and then has a lubricant effect on the system. The inset shows the interpenetration coefficient I between the brushes, calculated from

$$I = \int_0^{L_z/2} \rho_1(z)dz \Big/ \int_{-L_z/2}^{L_z/2} \rho_1(z)dz \qquad (18)$$

where $\rho_1(z)$ is the density profile of a single brush. As the brush chains are grafted onto the sliding surfaces, the interaction between the two brushes gives an important contribution to the friction. A strong correlation is observed between the brush interpenetration and the friction coefficient when the surface coverage is varying. We have previously established a similar correlation as a function of solvent quality. In bad solvent conditions, where no chains are detached, the polymer brushes are well-separated leading to a lower friction coefficient.[32] In the case of detached chains, even with $I = 0$, the system exhibits a dependence of the friction with respect to the surface coverage. This underlines the contribution of the free polymer chains to the frictional forces.

The rheology of the central region can be analysed by calculating the solvent viscosity. The profile of the shear viscosity η of the solvent can be calculated by

$$\eta(z) = -\frac{\langle p_{xz}(z)\rangle}{\nabla v_x(z)} \qquad (19)$$

where $v_x(z)$ is profile along z-axis of the x component of the solvent particles velocity. The velocity profile is fitted by using a 4-parameters sigmoid. Fig. 9a shows the solvent velocity profile for three surface coverages: $\rho_a = 0.911$, $\rho_a = 0.662$ and $\rho_a = 0.412$. The solvent particles are trapped inside the brushes and thus adopt a velocity profile similar to that of the grafted chains: the plateau at each extremity corresponds to the shear velocity

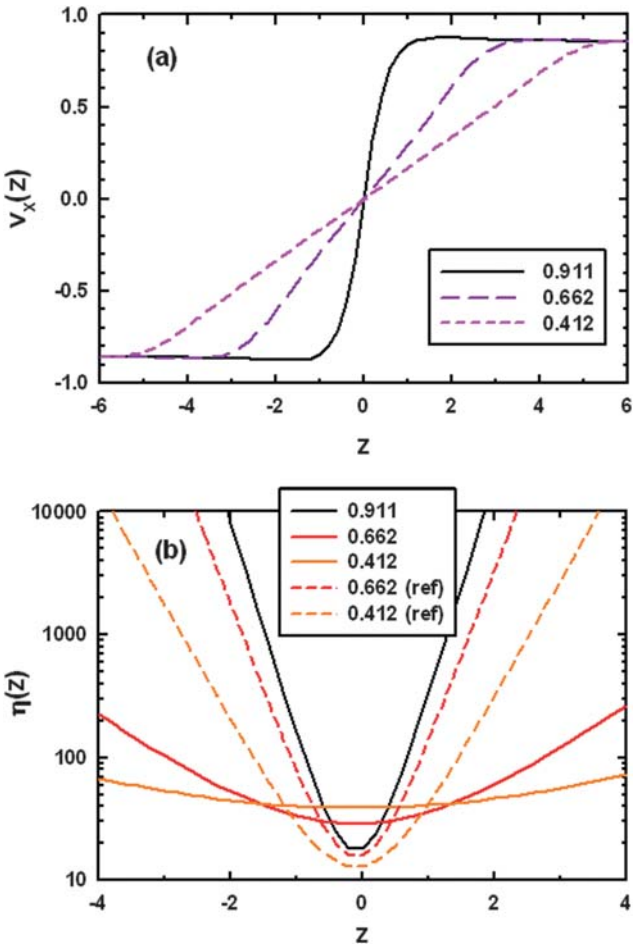

Fig. 9 (a) Profile of the x component of the solvent particles velocity along the normal z-axis. The solid, long-dash and dashed curves represent the systems with 0, 80 and 160 free chains, respectively. (b) Viscosity profile as a function of z for the system with no free chains (black curve). The solid red curve represents the system with 80 free chains ($\rho_a = 0.662$), and the solid orange curve represents the system with 160 free chains ($\rho_a = 0.412$). Dashed lines are shown from the corresponding reference system, in which the missing polymer chains are replaced by solvent particles (see section 2.3).

imposed by the solid surfaces. As more free chains are present in the central region, the brush influence is weakened and the velocity plateau is only present in the brush zone. The free chains region exhibits a linear velocity profile, which is a characteristic of a classical Newtonian fluid. Thus, the detachment of chains from the surface reduces the influence of the brushes in the middle of the box. The effect on the viscosity profile is shown in Fig. 9b for a few significant systems. Concerning the reference systems, the viscosity profile is very sharp due to the high value of the brush height which is maintained when decreasing the grafting density. In contrast, the local viscosity variation is smoother in the free chain zone due to the bulk behaviour of this phase.

Fig. 10 shows the values of the minimum solvent viscosity $\eta_{\min}$ calculated in the middle of the pore. The solvent viscosity of the reference systems decreases as the number of grafted chains decreases, as expected for a system that becomes richer in solvent particles. In the case of systems containing free chains, the

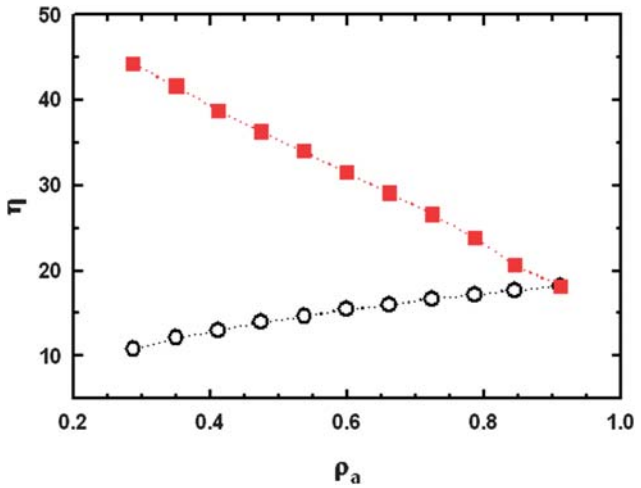

Fig. 10 Minimal solvent viscosity η_{min} as a function of the grafting density ρ_a in the middle of the box. Open circles represent the reference systems, in which the missing polymer chains are replaced by solvent particles (see section 2.3).

minimum solvent viscosity greatly increases as the central region becomes richer in polymer chains. A possible explanation is that the solvent is trapped in a polymer phase, which cause it to have less mobility. The increase is proportional to the number of detached polymer chains. Both friction and viscosity appear to be very sensitive to the presence of detached chains.

4 Conclusions

Dissipative particle dynamics is a powerful tool to model complex systems at the mesoscopic scale. We have used a simple model to simulate grafted polymer brushes under shear in the presence of free chemically identical polymer chains of identical length, immersed in a good solvent. We have developed a specific DPD methodology at constant-μVT with the addition of bond repulsions to model entangled polymers.

We have studied the dynamics of polymer chains as they detach from the grafted surface. The polymer chains are expelled from the brush and reach a free polymer region located in the center of the box. This new state is entropically favoured. The dynamics has two distinct regimes: the first is the chain's loss of memory of being previously grafted, and the second part is a diffusive behaviour inside the brush. The dynamics is not affected by removing the entanglement bond repulsions, which is in line with a reptation motion of the detached chains. Additionally, the absence of enthalpic effect when the chains are detached show that the dewetting of the brush is purely entropic which is in agreement with theory and experiments.

The central phase contains free polymer chains, which keeps the grafted chains away from each other. Thus, the polymer brushes shrink in the presence of free chains. The brush height of the reference systems is only slightly affected by the decrease of the grafting density and follows the expected scaling law. In the presence of free chains, the brush height becomes proportional to the grafting density, which increases the size of the free chain region. The penetration length of the polymer solution inside the brush follows the theoretical predictions for brush autophobicity behaviour.

The rheological properties are affected by this change in the structure. We have shown that the friction coefficient decreases linearly with the surface coverage when no detachment is considered. When few chains are expelled from the brush, the friction decreases significantly with the surface coverage and reaches an asymptotic value. A correlation between the interpenetration coefficient and the friction coefficient is determined from our mesoscopic simulations. It means that the detachment of polymer chains from grafted surfaces which may occur at high sliding velocities impacts significantly on the rheological properties of polymer brushes under shear.

Acknowledgements

This work was granted access to the HPC resources of IDRIS under the allocation 2009-i2009092119 made by GENCI (Grand Equipement National de Calcul Intensif).

References

1 A. Halperin, M. Tirrell and T. P. Lodge, *Adv. Polym. Sci.*, 1992, **100–1**, 31–71.
2 P. F. Luckham, *Adv. Colloid Interface Sci.*, 1991, **34**, 191–215.
3 S. S. Patel and M. Tirrell, *Annu. Rev. Phys. Chem.*, 1989, **40**, 597–635.
4 J. F. Brady and G. Bossis, *J. Fluid Mech.*, 1985, **155**, 105–129.
5 J. Klein, *Annu. Rev. Mater. Sci.*, 1996, **26**, 581–612.
6 J. Klein, E. Kumacheva, D. Mahalu, D. Perahia and L. J. Fetters, *Nature*, 1994, **370**, 634–636.
7 J. Klein, E. Kumacheva, D. Perahia and L. J. Fetters, *Acta Polym.*, 1998, **49**, 617–625.
8 H. J. Taunton, C. Toprakcioglu and J. Klein, *Macromolecules*, 1988, **21**, 3333–3336.
9 J. Klein, D. Perahia and S. Warburg, *Nature*, 1991, **352**, 143–145.
10 J. Klein, *Colloids Surf., A*, 1994, **86**, 63–76.
11 J. Klein, Y. Kamiyama, H. Yoshisawa, J. N. Israelachvili, G. H. Fredrickson, P. Pincus and L. J. Fetters, *Macromolecules*, 1993, **26**, 5552–5560.
12 A. N. Semenov, *Langmuir*, 1995, **11**, 3560–3564.
13 P. G. De Gennes, *Macromolecules*, 1980, **13**, 1069–1075.
14 S. T. Milner, *Science*, 1991, **251**, 905–914.
15 S. T. Milner, T. A. Witten and M. E. Cates, *Macromolecules*, 1988, **21**, 2610–2619.
16 P. G. De Gennes, *J. Phys.*, 1976, **37**, 1445–1452.
17 J. U. Kim and M. W. Matsen, *Eur. Phys. J. E*, 2007, **23**, 135–144.
18 K. Kremer and G. S. Grest, *J. Chem. Phys.*, 1990, **92**, 5057–5086.
19 M. Pütz, K. Kremer and G. S. Grest, *Europhys. Lett.*, 2000, **49**, 735–741.
20 M. Murat and G. S. Grest, *Phys. Rev. Lett.*, 1989, **63**, 1074–1077.
21 G. S. Grest, *Macromolecules*, 1994, **27**, 418–426.
22 G. H. Peters and D. J. Tildesley, *Phys. Rev. E: Stat. Phys., Plasmas, Fluids, Relat. Interdiscip. Top.*, 1995, **52**, 1882–1890.
23 G. S. Grest, *Adv. Polym. Sci.*, 1999, **138**, 149–183.
24 G. S. Grest, *Curr. Opin. Colloid Interface Sci.*, 1997, **2**, 271–277.
25 P. S. Doyle, E. S. G. Shaqfeh and A. P. Gast, *Macromolecules*, 1998, **31**, 5474–5486.
26 P. S. Doyle, E. S. G. Shaqfeh and A. P. Gast, *Phys. Rev. Lett.*, 1997, **78**, 1182–1185.
27 I. M. Neelov, O. V. Borisov and K. Binder, *Macromol. Theory Simul.*, 1998, **7**, 141–156.
28 M. G. Saphiannikova, V. A. Pryamitsyn and T. Cosgrove, *Macromolecules*, 1998, **31**, 6662–6668.
29 I. M. Neelov, O. V. Borisov and K. Binder, *J. Non-Cryst. Solids*, 1998, **235–237**, 731–736.
30 T. Kreer, M. H. Müser, K. Binder and J. Klein, *Langmuir*, 2001, **17**, 7804–7812.
31 P. Malfreyt and D. J. Tildesley, *Langmuir*, 2000, **16**, 4732–4740.

32 D. Irfachsyad, D. J. Tildesley and P. Malfreyt, *Phys. Chem. Chem. Phys.*, 2002, **4**, 3008–3015.
33 C. Pastorino, K. Binder and M. Müller, *Macromolecules*, 2009, **42**, 401–410.
34 A. Chakrabarti, P. Nelson and R. Toral, *J. Chem. Phys.*, 1994, **100**, 748–749.
35 J. Luettmer-Strathmann, F. Rampf, W. Paul and K. Binder, *J. Chem. Phys.*, 2008, **128**, 064903.
36 A. J. Masters and P. B. Warren, *Europhys. Lett.*, 1999, **48**, 1–7.
37 P. J. Hoogerbrugge and J. M. V. A. Koelman, *Europhys. Lett.*, 1992, **19**, 155–160.
38 F. Goujon, P. Malfreyt and D. J. Tildesley, *ChemPhysChem*, 2004, **5**, 457.
39 F. Goujon, P. Malfreyt and D. J. Tildesley, *Mol. Phys.*, 2005, **103**, 2675–2685.
40 F. Goujon, P. Malfreyt and D. J. Tildesley, *J. Chem. Phys.*, 2008, **129**, 034902.
41 F. Goujon, P. Malfreyt and D. J. Tildesley, *Macromolecules*, 2009, **42**, 4310–4318.
42 M. Müller and L. G. MacDowell, *Europhys. Lett.*, 2001, **55**, 221–227.
43 B. Widom, *J. Chem. Phys.*, 1963, **39**, 2808–2812.
44 G. H. Peters and D. J. Tildesley, *Phys. Rev. E: Stat. Phys., Plasmas, Fluids, Relat. Interdiscip. Top.*, 1996, **54**, 5493–5501.
45 A. M. Skvortsov, A. A. Gorbunov, F. A. M. Leermakers and G. J. Fleers, *Macromolecules*, 1999, **32**, 2004–2015.
46 L. G. MacDowell and M. Müller, *J. Phys.: Condens. Matter*, 2005, **17**, S3523–3528.
47 M. W. Matsen, *J. Chem. Phys.*, 2002, **117**, 2351–2358.
48 M. W. Matsen and J. M. Gardiner, *J. Chem. Phys.*, 2001, **115**, 2794–2804.
49 L. G. MacDowell and M. Müller, *J. Chem. Phys.*, 2006, **124**, 084907.
50 C. Pastorino, K. Binder, T. Kreer and M. Müller, *J. Chem. Phys.*, 2006, **124**, 064902.
51 M. Aubouy, J. L. Harden and M. E. Cates, *J. Phys. II*, 1996, **6**, 969–984.
52 K. Binder, P.-Y. Lai and J. Wittmer, *Faraday Discuss.*, 1994, **98**, 97–109.
53 R. D. Groot and P. B. Warren, *J. Chem. Phys.*, 1997, **107**, 4423–4435.
54 P. Español and P. B. Warren, *Europhys. Lett.*, 1995, **30**, 191–196.
55 R. D. Groot and K. L. Rabone, *Biophys. J.*, 2001, **81**, 725–736.
56 F. Müller-Plathe, *ChemPhysChem*, 2002, **3**, 754–769.
57 J. Baschnagel, K. Binder, P. Doruker, A. A. Gusev, O. Hahn, K. Kremer, W. L. Mattice, F. Müller-Plathe, M. Murat, W. Paul, S. Santos, U. W. Suter and V. Tries, *Adv. Polym. Sci.*, 2000, **152**, 41–156.
58 J. T. Padding and W. J. Briels, *J. Chem. Phys.*, 2002, **117**, 925–943.
59 B. M. Forrest and U. W. Suter, *J. Chem. Phys.*, 1995, **102**, 7256–7266.
60 R. Chang, G. S. Ayton and G. A. Voth, *J. Chem. Phys.*, 2005, **122**, 244716.
61 Y. Kong, C. W. Manke, W. G. Madden and A. G. Schlijper, *Int. J. Thermophys.*, 1994, **15**, 1093–1101.
62 A. G. Schlijper, P. J. Hoogerbrugge and C. W. Manke, *J. Rheol.*, 1995, **39**, 567–579.
63 S. Kumar and R. G. Larson, *J. Chem. Phys.*, 2001, **114**, 6937–6941.
64 S. P. Holleran and R. G. Larson, *Rheol. Acta*, 2008, **47**, 3–17.
65 B. Widom, *J. Stat. Phys.*, 1978, **19**, 563–574.
66 J. G. Powles, S. E. Baker and W. A. B. Evans, *J. Chem. Phys.*, 1994, **101**, 4098–4102.
67 J. G. Powles, W. A. B. Evans and N. Quirke, *Mol. Phys.*, 1982, **46**, 1347–1370.
68 J. G. Powles, B. Holtz and W. A. B. Evans, *J. Chem. Phys.*, 1994, **101**, 7804–7810.
69 G. Reiter and R. Khanna, *Phys. Rev. Lett.*, 2000, **85**, 5599–5602.
70 C. Gay, *Macromolecules*, 1997, **30**, 5939–5943.
71 Y. Katsumoto, F. Tsunomori, H. Ushiki, L. Letamendia and J. Rouch, *Eur. Polym. J.*, 2001, **37**, 475–483.
72 P. G. Ferreira, A. Ajdari and L. Leibler, *Macromolecules*, 1998, **31**, 3994–4003.
73 J. H. Irving and J. G. Kirkwood, *J. Chem. Phys.*, 1950, **18**, 817–829.
74 J. P. R. B. Walton, D. J. Tildesley, J. S. Rowlinson and J. R. Henderson, *Mol. Phys.*, 1983, **48**, 1357–1368.
75 H. A. Barnes, J. F. Hutton, K. Walters, *An Introduction to Rheology*, Elsevier, Amsterdam, 1989.